6-2007

Fluctuating Two-state Light Harvesting In A Photosynthetic Membrane

Duohai Pan

Dehong Hu

Ruchuan Liu

Xiaohua Zeng

Samuel Kaplan

See next page for additional authors

Author(s)
Duohai Pan, Dehong Hu, Ruchuan Liu, Xiaohua Zeng, Samuel Kaplan, and H. Peter Lu

Fluctuating Two-State Light Harvesting in a Photosynthetic Membrane†

Duohai Pan,‡ Dehong Hu,‡ Ruchuan Liu,‡ Xiaohua Zeng,§ Samuel Kaplan,§ and H. Peter Lu*,‡,⊥

Fundamental Science Directorate, Pacific Northwest National Laboratory, P.O. Box 999, Richland, Washington 99352, Department of Microbiology and Molecular Genetics, The University of Texas Health Science Center, Medical School, 6431 Fannin, Houston, Texas 77030, Center for Photochemical Sciences, Department of Chemistry, Bowling Green State University, Bowling Green, Ohio 43403

Received: February 22, 2007; In Final Form: April 30, 2007

The mechanism by which light is converted into chemical energy in a natural photosynthetic system has drawn considerable research interest. Using fluorescence spectroscopy and microscopic imaging, we have observed fluctuating intermolecular protein fluorescence resonant energy transfers (FRET) among light-harvesting proteins I and II (LH1 and LH2) in bacterial photosynthetic membranes. Using two-channel, FRET, photon-counting detection and a novel, two-dimensional cross-correlation function amplitude-mapping analysis, we revealed fluorescence intensity and spectral fluctuations of donor (LH2) and acceptor (LH1) fluorescence involving FRET. Our results suggest that there are dynamic coupled and noncoupled states of the light-harvesting protein assemblies in photosynthetic membranes. The light-harvesting complex assembly under ambient conditions and under water involves dynamic intermolecular structural fluctuations that subsequently disturb the degree of energy transfer coupling between proteins in the membrane. Such intrinsic and dynamic heterogeneity of the native photosynthetic membranes, often submerged under the overall thermally induced spectral fluctuations and not observable in an ensemble-averaged measurement, likely plays a critical role in regulating the light-harvesting efficiency of the photosynthetic membranes.

Introduction

How light is converted into chemical energy in a natural photosynthetic system is of great interest in energy sciences and fundamental physical chemistry. Purple bacteria typically contain two types of light-harvesting (LH) membrane protein complexes, LH1 and LH2.[1,2] A reaction center is surrounded by a donut-shaped LH1 complex protein, and multiple LH2 complexes peripherally surround the LH1 in a two-dimensional assembly.[1,2] The initial event in photosynthesis is the photon excitation of an LH2, followed by rapid and efficient energy transfer to LH1 and then to the reaction center, where a charge separation takes place.[1−3] In a photosynthetic membrane, LH2 has two absorption bands at 800 and 850 nm; whereas the LH1 has a lower-energy absorption band at 875 nm. Studies on the static protein structures,[2] static protein assembly structures in membranes,[1,4] ensemble-averaged energy transfer dynamics,[5−9] and single-molecule LH2 spectroscopic studies[10−13] have provided extensive knowledge on photosynthesis, although static structure studies reveal photosynthetic membrane features in an organized LH1−LH2 assembly; however, there has been no report of the interprotein energy transfer fluctuating coupling of the assembly in a native photosynthetic membrane under ambient conditions.[1,4,7,8] The intermolecular energy-transfer coupling among LH2 and LH1 proteins is critical for understanding the light-harvesting mechanism and dynamics because the light energy conversion can occur only when the LH1−LH2 energy transfer is active.

† Part of the special issue "Kenneth B. Eisenthal Festschrift".

* Corresponding author. E-mail: hplu@bgsu.edu.
‡ Pacific Northwest National Laboratory.
§ The University of Texas Health Science Center, Medical School.
⊥ Bowling Green State University.

The mechanism of the energy transfer will be dramatically different if the LH1−LH2 energy transfer efficiency is constant or if there are fluctuations in LH2−LH2 and LH1−LH2 energy transfer coupling in the photosynthetic membranes during the light-harvesting process. It is understandable that the diffusional motions of the light-harvesting proteins are essentially confined in the photosynthetic membranes. Nevertheless, the energy transfer coupling is not necessarily constant and static and can be significantly disrupted by thermal motions of the membranes and proteins, because the energy transfer coupling is highly sensitive to the distance and orientations of the transition dipoles of the light-harvesting proteins. However, the knowledge about the temporal fluctuations of the energy transfer coupling is insufficient, since the fluctuations cannot be readily observed in conventional ensemble-averaged measurements.

This article focuses on the intermolecular energy transfer of LH2−LH1 complexes in photosynthetic membranes under buffer solution. Using fluorescence spectroscopy and microscopic imaging, we have studied the native photosynthetic membranes, LH2-knocked-out mutant membranes, and LH1-knocked-out mutant membranes from purple bacteria of *Rhodobacter* (*Rb.*) *sphaeroides*. We have observed fluctuating intermolecular protein energy transfers in bacterial photosynthetic membranes by two-channel fluorescence photon-counting selectively for LH2 and LH1 emissions. Our results suggest that there are dynamic coupled and noncoupled states of the light-harvesting protein assemblies in photosynthetic membranes. The energy transfer fluctuation, where the donor−acceptor intensity is anticorrelated, is often submerged in the overall thermally induced spectral fluctuation, where the donor−acceptor intensity is autocorrelated. We have demonstrated a new two-dimensional

10.1021/jp071493y CCC: $37.00
Published on Web 05/31/2007

autocorrelation amplitude mapping analysis to identify the intermittent energy transfer coupling.

Experimental Section

Confocal Fluorescence Microscopy. The fluorescence spectra and images were acquired with an inverted confocal microscope (Axiovert-200, Zeiss). The excitation source was a tunable Ti:sapphire laser system (Coherent, Mira 900F) producing 795-nm, 100-fs pulses with a repetition of 76 MHz. The laser power was 1−5 μW, with the laser beam reflected by a dichroic beam splitter (815 dclp, Chroma Technology) and focused by a high-numerical-aperture objective (1.3 NA, 100×, Zeiss) on the sample surface at a diffraction-limited spot of ~300-nm diameter. The sample solution was mixed with 1% agarose gel (99% water), heated just above the gelling temperature (26 °C). A 10-μL sample of agarose solution was dropped and sandwiched between two clean cover slips. The sample could be raster-scanned or positioned with respect to the laser focus by using an *x*-*y* electropiezo, closed-loop, position-scanning stage (Physik Instrumente). The fluorescence emission was collected by the same microscopic objective and filtered with a long-pass filter (Chroma Technology).

To obtain fluorescence images and intensity traces, the emission was split by a dichroic beam splitter (875 dclp) into two color beams at 860 and 890 nm. The two-channel signals were imaged by a pair of Si avalanche photodiode single-photon-counting modules (SPCM-AQR-16, Perkin-Elmer Optoelectronics) for detecting fluorescence. Trajectories were detected in intervals of 10 ms for each time bin by using homemade photon time-stamping electronics.[14,15] A typical image was acquired by continuously raster-scanning the sample over the laser focus with a scanning speed of 4 ms/pixel, with each image being 100 pixels × 100 pixels. After the coordinates of the photosynthetic membrane fragments were determined, the piezo stage was positioned to bring the fragments, often formed vesicle particles, into the laser focus of the objective to record the intensity trajectories or fluorescence spectra. Fluorescence spectra were detected with a N2-CCD (Spec 10: 400BR, Roper Scientific) coupled to an imaging monochromator (Acton 150, Acton Research). A series of fluorescence spectra were consecutively collected with an integration time of 0.1 s. All measurements were carried out in an oxygen-free environment under N_2 at room temperature.

Bacterial Growth and Sample Preparation. Intracytoplasmic membrane vesicles (ICMs) from photosynthetic membranes of *Rb. sphaeroides*[16] were used in our experiments. *Rb. sphaeroides* 2.4.1 was grown photosynthetically at a light intensity of 100 W/m^2 with sparging in a gas mixture of 95% N_2 and 5% CO_2, and cells were harvested at 0.5 A_{600nm}. ICMs were separated on a Sepharose 2B column (50 × 2.0 cm), and were further purified by rate-zonal sucrose gradient centrifugation at 63 500*g* for 10 h. Membranes were isolated following ultracentrifugation at 260 000*g* for 1.0 h. The isolated membranes were then dissolved in 20 mM Tris−HCl at pH 8.0 containing 100 mM NaCl and 1% lauryl *N*,*N*-dimethylamine-*N*-oxide for the isolation of spectral complexes, as described previously,[17,18] by DEAE-52 cellulose chromatography and 20−40% sucrose gradient centrifugation at 260 000 for 16 h at 4 °C. The spectral complexes were collected by measuring the spectral absorption at 800 and 850 nm. Purified ICM vesicles and LH2 complexes were stored at −80 °C.

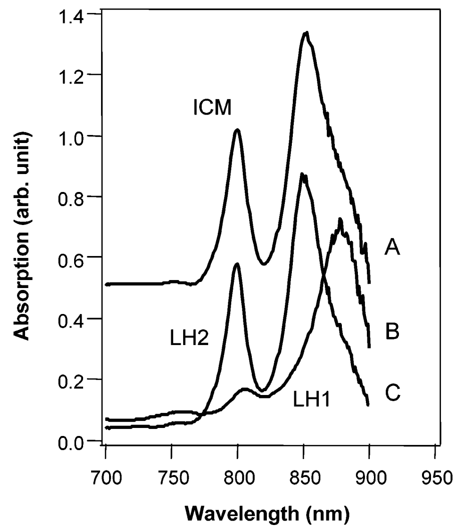

Figure 1. The absorption spectra of native photosynthetic membranes (ICM) and truncated membranes deleting LH2 and LH1, respectively. (A) Native membrane containing both LH2 and LH1 protein complexes. Both absorption bands at 800 and 850 nm for LH2, and at 870 nm for LH1 are observable. Its baseline was shifted up for clear view. (B) LH2 deleted membrane containing only LH1 complex. Only a dominated LH1 absorption band is observed at 876 nm. (C) LH1 deleted membrane containing only LH2 complex. Only the LH2 absorption bands of B800 and B850 are observed at 800 and 850 nm.

Results and Discussion

Ensemble-averaged near-IR absorption spectrum (Figure 1) of the native membrane together with the spectra of truncated membranes deleting the LH1 or LH2 complexes clearly show that the light-harvesting complex proteins dominate the membrane spectrum. The spectrum of the membrane deleting the LH2 complex exhibits a single broad band at 876 nm, corresponding to the B875 ring in the LH1 complex.[3−5] The spectrum of the membrane deleting the LH1 complex has two main bands, the B800 ring at 800 nm and the B850 ring at 850 nm in the LH2 complex.[4−7]

To estimate the number density of the LH2 and LH1 proteins in our photosynthetic membrane fragments, we obtained the single vesicle fluorescence images of the membrane fragments on a glass surface under water. The confocal fluorescence image in Figure 2A was obtained by imaging the fluorescence at 880 nm with a raster-scanning, 795-nm laser excitation. Figure 2B presents the statistical analysis of the 185 single imaging spots at 880-nm wavelength, and the distribution shows a single peak of dominated photon counts at 90 ± 40 ct/ms. There are also a few much smaller peaks at higher counting rates that are essentially the multiples of the major distribution peak. The single dominated distribution of fluorescence count rates suggests that most imaging fragments monitored were single intracytoplasmic vesicles, rarely appearing in aggregate vesicles or adjacent membranes. On the basis of the extinction coefficient at the B850 band ($\epsilon_{850} = 96$ mM cm^{-1}),[3] the concentration of LH2 in the solution for the fluorescence imaging measurement is 1.2 nM. For a 10-μL agarose solution sample sandwiched between two clean cover slips (25 mm × 25 mm), our imaging measurements typically observed about 19 single vesicles per image (15 μm × 15 μm). We estimated that, on an average, there are ~130 LH2 proteins in each vesicle.

The fluorescence spectrum of a single vesicle (Figure 3A) shows two fluorescence bands at 860 and 890 nm, and they have been attributed to the LH2 excited-state emission and the excitation-hopping from LH2 to LH1 through energy transfer,

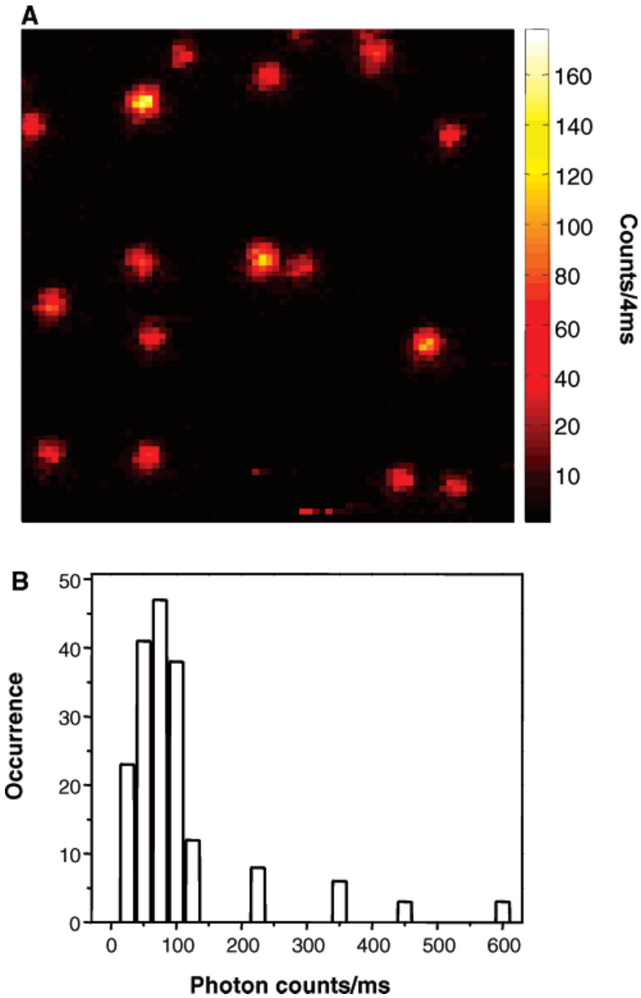

Figure 2. Optical measurements for the individual native and intact photosynthetic membranes of *Rb. sphaeroides*. (A) Fluorescence image of single native intracytoplasmic membrane vesicles (ICM). (B) Statistical analysis of the 185 single imaging spots. The distribution of fluorescence count rates reflects that each imaging feature contains an individual intracytoplasmic vesicle.

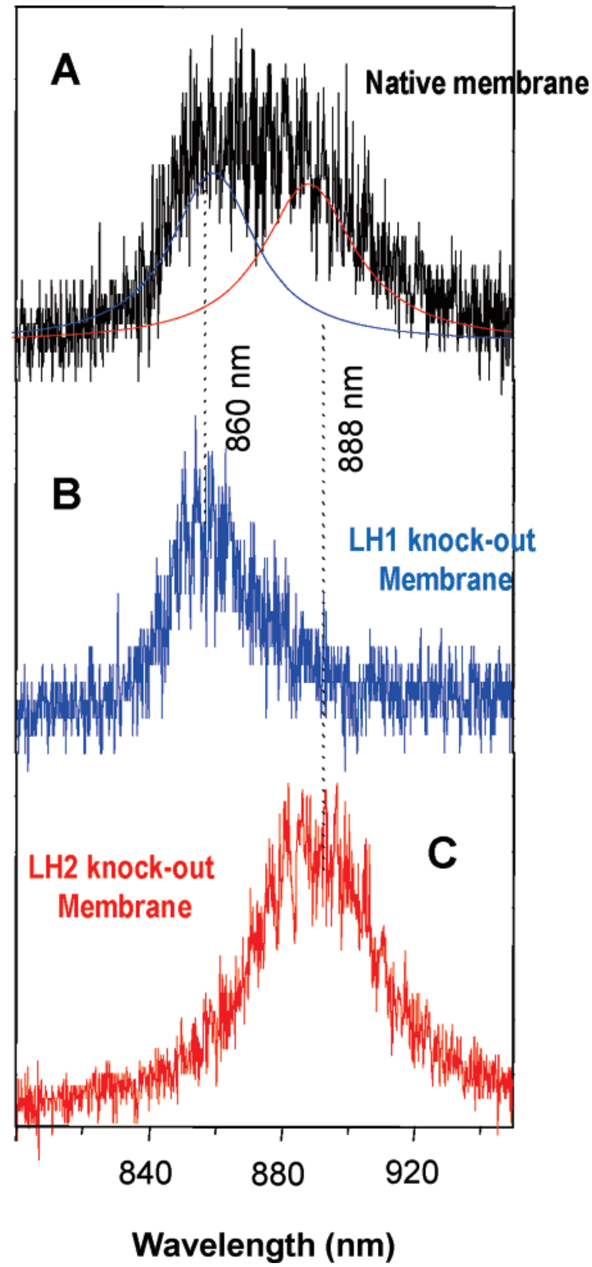

Figure 3. Emission spectra of photosynthetic membranes of *Rb. sphaeroides*. (A) A typical fluorescence spectrum of a single wild-type ICM. (B, C) fluorescence spectra of a single truncated ICM deleting LH1 and LH2, respectively. (A) Native membrane containing both LH2 and LH1 protein complexes. Both emission bands at 860 and 885 nm for LH2 and LH1, respectively, are observable. (B) LH1 knocked-out membrane containing only LH2 complex. Only the LH2 emission band is observed at 860 nm. (C) LH2 knocked-out membrane containing only the LH1 complex. Only the LH1 emission band is observed at 885 nm.

respectively.[5] Figure 3B and C shows the emission spectra from single truncated vesicles, deleting LH1 and LH2, respectively. The emission peaks are consistent with the literature and with our assignment of LH2 and LH1 bands in Figure 3A.

Energy transfer of light-harvesting proteins regulates the overall solar energy conversion efficiency of photosynthetic membranes, and the energy transfer can be probed by measuring the fluorescence spectra of the proteins, such as fluorescence resonant energy transfer (FRET) spectroscopic measurements. To characterize the intermolecular energy transfer among LH2 and LH1 proteins in the membranes, we collected a series of consecutive fluorescence spectra from the native photosynthetic membrane fragments under buffer solution and ambient condition. Figure 4A shows a portion of a typical trajectory of consecutive fluorescence spectra from a single ICM vesicle of a photosynthetic membrane fragment at 50 ms spectral collection time for each spectrum. We have calculated the mean and standard deviation of each spectrum along the spectral time trajectories. Figure 4B shows a trajectory of the consecutive spectral means and the standard deviation of the spectral means. Spectral peak position, associated with the spectral mean, has shown significant fluctuation as large as 300 cm^{-1} beyond a measurement error bar of $\pm$30 cm^{-1}. We have analyzed the spectral fluctuation dynamics by autocorrelation function calculated from the time trajectories of the spectral means, and the result is given by

$$C(t) = <\Delta M(t)\, \Delta M(0)>$$

where $M(t)$ is the spectral mean changing with time, and $\Delta M(t) = M(t) - <M(0)>$, i.e., $\Delta M(t)$ is the spectral mean fluctuation from the average spectral mean of the entire trajectory, $<M(0)>$. Figure 4C shows an autocorrelation function calculated from the trajectory in Figure 4B, and a 1.26-s spectral fluctuation time is revealed from the analysis. Although the time resolution of the spectral fluctuation is limited by the spectral collection

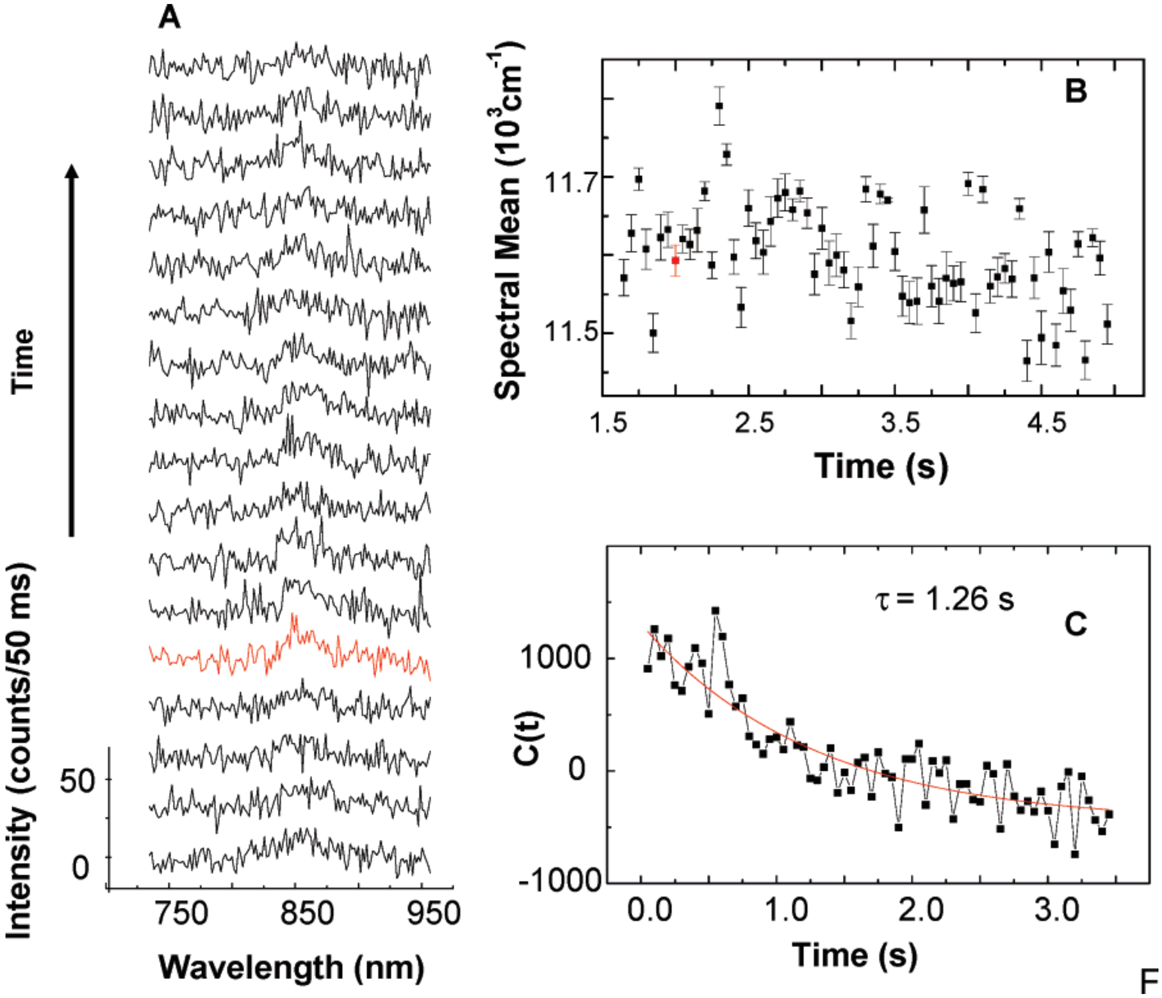

Figure 4. Single wild-type ICM emission spectral fluctuation. (A) A portion of a spectral trajectory consecutively recorded with 50-ms collection time for each spectrum. (B) Spectral mean trajectory calculated from the experimental spectral trajectory in (A); the red highlighted data point is calculated from the red highlighted spectrum in A. The error bars are standard deviations calculated from each spectrum in A. (C) Autocorrelation function calculated from spectral mean trajectory in B. An exponential decay of 1.26 s reflects the spectral fluctuation rate.

time of 50 ms, yet we were able to detect the slow spectral fluctuation down to the second time scale.

To have a higher time resolution in the measurements and further investigate the physical nature of the fluorescence spectral fluctuation, we have specifically probed the intensity fluctuations of the two bands in the vesicle spectra at 860 and 890 nm associated with LH2 and LH1 proteins, respectively. We used two-channel single-photon-counting detection measurements[15,16] at 860 and 890 nm to collect the intensity fluctuation time trajectories for each of the two bands simultaneously, $I'_1(t)$ and $I'_2(t)$ (Figure 5).

To reveal the FRET spectral fluctuation, we have calculated a two-dimensional, cross-correlation function amplitude distribution, a novel analysis of the spectral fluctuation dynamics (Figure 7). In this analysis, a variable start time and a variable end time, t_{start} and t_{stop}, were chosen to calculate the autocorrelation function from the two-channel signal intensity time trajectories. The two variable parameters, start time and end time, define the start time and the time lapse of a cross-correlation function calculation window along a two-band fluorescence intensity trajectory. This 2-D calculation gives a cross-correlation for a pair of segments from t_{start} to t_{stop} as

$$I'_1(t),\quad I'_2(t):$$

$$C(\tau, t_{start}{:}t_{stop}) = \int_{t_{start}}^{t_{stop}} I'_1(t) I'_2(t-\tau)\, dt$$

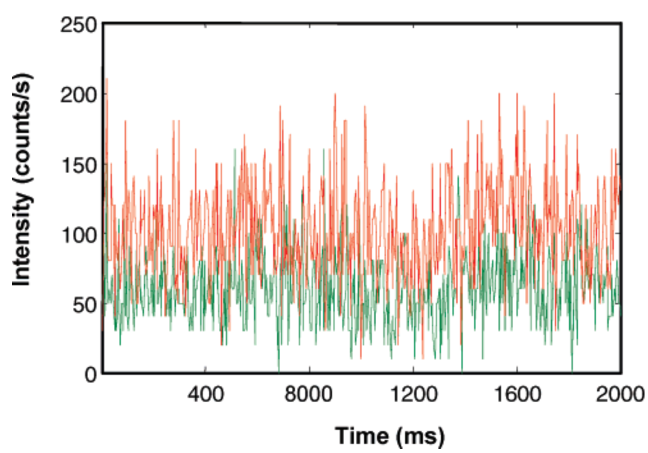

Figure 5. A pair of fluorescence intensity trajectories of LH1 ($I_1(t)$, red curve) and LH2 ($I_2(t)$, green curve). The emission photon signal was split at 875 nm, recording the red curve at >875 nm for the LH1 signal and the green curve at <875 nm for the LH2 signal.

The window of t_{start} to t_{stop} was scanned in a range through the intensity trajectories. The initial amplitude of C(τ, t_{start}:t_{stop}) was presented by the difference between the first n points and the next $n + m$ points on both sides of $\tau = 0$.

$$A = \{<C(1{:}n)> + <C(-1{:}-n)>\} - \{<C(n+1{:}n+m)> + <C(-(n+1){:}-(n+m))>\}$$

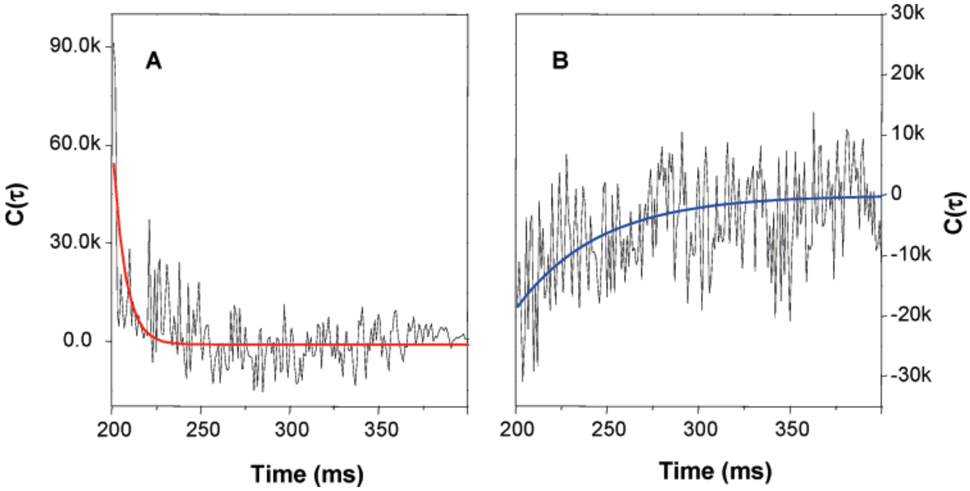

Figure 6. Cross-correlation functions calculated from experimental trajectories of LH1 ($I_1(t)$) and LH2 ($I_2(t)$), at 890 and 860 nm, respectively. (A) A typical cross-correlation function with a positive amplitude calculated from a pair of intensity trajectories, $I_1(t)$ and $I_2(t)$, with correlated fluctuations. (B) A typical cross-correlation function with a negative amplitude from a pair of intensity trajectories, $I_1(t)$ and $I_2(t)$, with anti-correlated fluctuations.

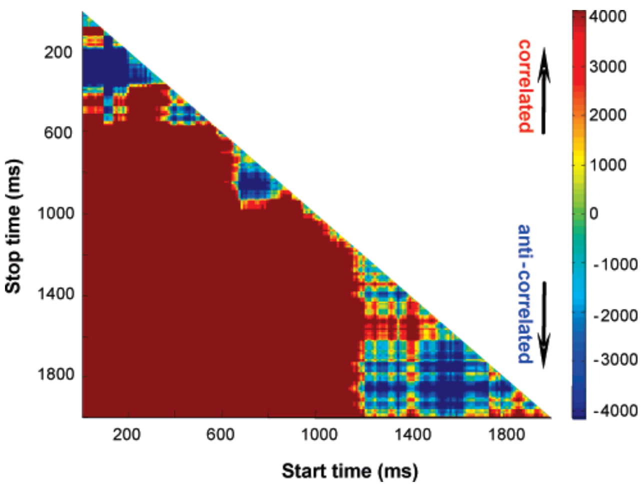

Figure 7. Two-dimension, cross-correlation function amplitude distribution. The hot color represents positive amplitude, and the cold color represents negative amplitude. The correlated function (Figure 6A) is calculated between the 860- and 890-nm bands from the start time of 600 ms to the stop time of 800 ms, and the anti-correlated function (Figure 6B) is calculated between the two bands from the start time of 200 ms to the stop time of 400 ms.

The index n and m defined the precision of calculated initial amplitude, A, of the correlation function. In our analysis, we chose $n = m = 10$, which is sufficient to obtain a reliable calculation of A. As a function of t_{start} and t_{stop}, the value of A is plotted as a two-dimensional map of t_{start} and t_{stop}. A hot color represents positive amplitude of $C(\tau)$ and a cold color represents negative amplitude of $C(\tau)$. Positive amplitude A indicates correlation $C(\tau, t_{start}:t_{stop})$, and negative amplitude A indicates anti-correlation $C(\tau, t_{start}:t_{stop})$.

If the intensity trajectories of $I'_1(t)$ and $I'_2(t)$ are completely dominated by LH2−LH1 energy transfer, the intensities of the two bands from LH2 and LH1 should have an anticorrelated fluctuation characterized by a negative amplitude of cross-correlation functions (such as in Figure 6B). On the other hand, if the thermally induced spectral fluctuation dominates, the intensity fluctuation of the two channels will be noncorrelated or correlated with positive amplitude of the cross-correlation functions (Figure 6A). In real measurements under room temperature, the light-harvesting complexes and associated photosynthetic membranes always involve a certaindegree of thermally induced spectral fluctuations, fluctuation due to photobleaching of LH2 and LH1 proteins, and LH2−LH2 homo-energy-transfer-induced intensity fluctuations. Consequently, there is always a component of positive amplitude of cross-correlation functions. The complexity of picking up the FRET-related fluorescence intensity fluctuation, the negative amplitude of the cross-correlation, will depend on the relative amplitude of both FRET-associated and thermally induced spectral fluctuations. Using conventional one-dimensional, cross-correlation analysis (Figure 6A and B), the overall signal-to-noise ratio of the calculated cross-correlation function is low. The real FRET spectral fluctuation was often buried under a high thermally induced spectral fluctuation background.

To extract the energy transfer process swamped by large thermally induced spectral fluctuation, our 2-D cross-correlation amplitude mapping analysis is powerful. Our experimental data showed that although over the whole trajectory, the correlation amplitude is positive, there are some time windows showing negative correlation amplitude. Figure 7 shows both positively and negatively correlated functional amplitude by region, corresponding to correlated and anti-correlated fluctuations (for example, as shown in Figure 6A and B). The anti-correlated fluorescence fluctuation (Figure 6B) indicates dynamic heterogeneity in the spatial structure of the LH1 and LH2 assembly in a photosynthetic membrane, reflecting the intermolecular energy transfer and the temporal variations of intermolecular energy transfer efficiency between LH2 and LH1. The overall thermal fluctuation of the membrane gives the correlated two-band fluctuation background (Figure 7), whereas the optical coupling of LH2 and LH1 involves fluctuation between two states, one dominated by energy transfer (anti-correlated two-band fluctuation) and the other dominated by thermal fluctuation (correlated two-band fluctuation). In the 2-D distribution, the existence of regions of correlated and anti-correlated functions is not dependent on the intensity of the laser excitation but is, instead, an intrinsic property. The intermittent anti-correlated fluctuation can be well-identified by our 2-D cross-correlation amplitude mapping analysis (Figure 7), a valid and effective approach to search for a subset anti-correlated fluctuation that cannot be revealed in the conventional correlation analysis. We have observed similar intermittent anti-correlated fluctuations in the 2-D correlation function amplitude distributions for about 10% of single membrane vesicles.

The significant advantage of the 2-D correlation function amplitude mapping is that both the correlated and anti-correlated

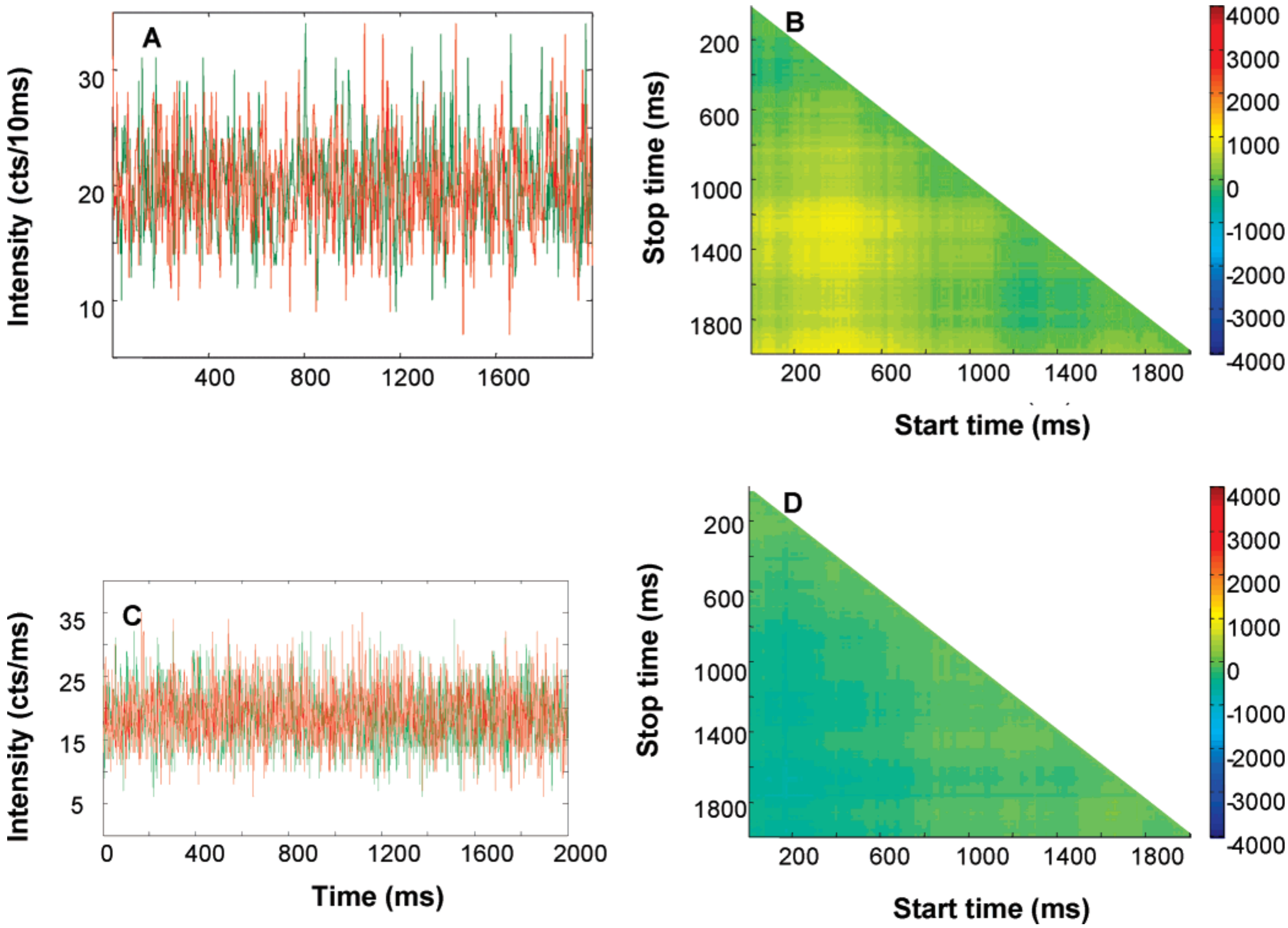

Figure 8. Analysis of simulated and experimental white-noise trajectories. Two-dimension, cross-correlation function amplitude distributions calculated from (A) a pair of simulated white noise trajectories and (C) a pair of experimentally collected room-light intensity trajectories showing neither significant positive nor negative correlation function amplitudes (B, D).

spectral intensity fluctuations can be identified pixel-by-pixel on the basis of the calculated cross-correlation function pixel-by-pixel. Specifically, (1) the parameter of the Z-axis is the amplitude of the cross-correlation function from FRET donor−acceptor two-channel emission intensity time trajectories. A positive amplitude means (represented by a hot color) that the two intensity trajectories, $I_1(t)$ and $I_2(t)$, fluctuate in the correlated way (both go up and down together); whereas, a negative amplitude (represented by a cold color) means that the two intensity trajectories, $I_1(t)$ and $I_2(t)$, fluctuate in the anti-correlated way (one goes up while the other one goes down, and vise versa). A zero amplitude (represented by a green color) means that the two intensity $I_1(t)$ and $I_2(t)$ fluctuate randomly without a correlation. (2) The parameters of the $X-Y$ axes represent the time window between t_{start} and t_{stop} for calculating the cross-correlation functions from the FRET donor−acceptor two-channel emission intensity time trajectories. The t_{start} and t_{stop} of the 2D cross-correlation amplitude map define the time window (position and width) for the calculated cross-correlation function, and the width and position of the window are scanned through the intensity trajectories by scanning all the possible values of t_{start} and t_{stop}.

To further validate the analysis, we calculated a 2-D correlation function amplitude map (Figure 8B and D) from both simulated white noise trajectories (Figure 8A) and experimental white noise trajectories (Figure 8C) recorded from room light. There is no observable anti-correlated or correlated fluctuation at an amplitude scale beyond error bars, which suggests that

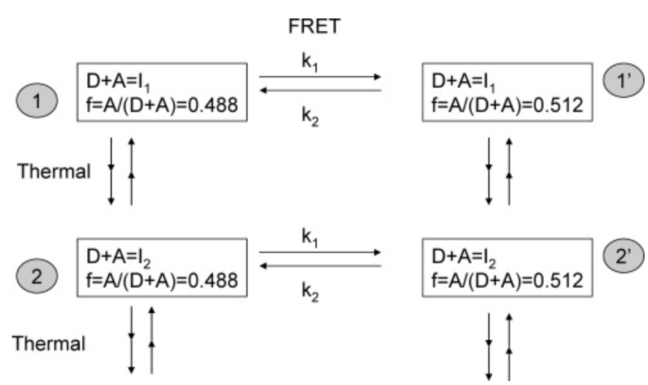

Figure 9. A kinetic model of spectral fluctuation of photosynthetic membrane ICM fragment, associated with both FRET-related and thermally induced spectral fluctuations. In this model, the fluctuation dynamics of each channel (channel 1, 2, ...) is single-exponential with rate of $k_1 + k_2$ between states 1 and 1′ (2 and 2′, ...). States 1 and 1′ involve a different energy transfer efficiency of FRET. Different channels have different overall fluorescence intensities (I_1, I_2, ...) perturbed by thermal fluctuations. The thermo-driven interconversion dynamics among the channels (channel 1, 2, ...) are modeled as Lévy flight diffusion dynamics, and the fluctuation rate of energy transfer efficiency change (1 and 1′, 2 and 2′, ...) is modeled as first-order kinetics k_1 and k_2. Here, $I = A + D$, where D and A represent the fluorescence intensities of the FRET donor and acceptor, and ξ (= $A/(A + D)$) represents the FRET efficiency.

the anti-correlated fluctuation revealed in Figure 7 originates from the intrinsic energy transfer property between the LH2

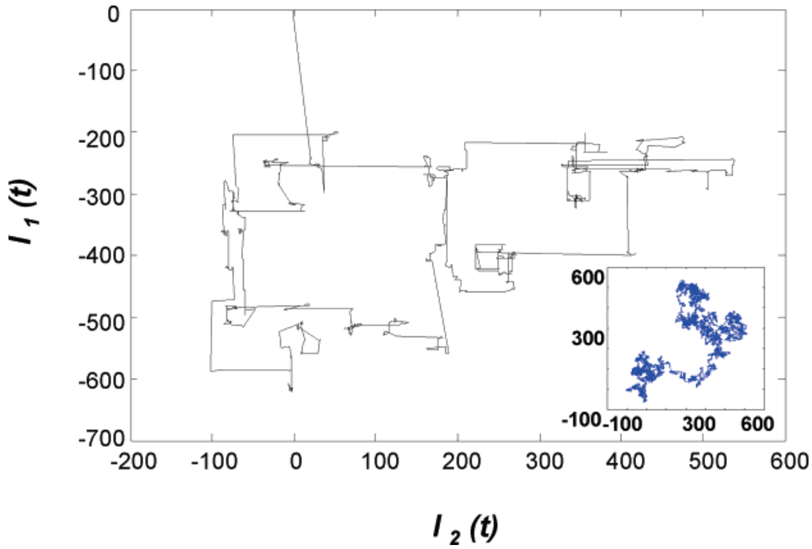

Figure 10. An illustration of Lévy flight. The simulated Lévy flight is generated by a pair of trajectories that the jump size obeys, $p(x) = 1/\pi(1 + x^2)$. Inset: simulated 2-dimension Brownian diffusion by generating a pair of trajectories with the jump size obeying Gaussian distribution.

and LH1 complexes in the native membrane. The FRET spectral two-band anti-correlated fluctuation appeared intermittently beyond the background of uncorrelated noise.

To explore the mixed spectral two-band correlated thermal spectral fluctuation and anti-correlated FRET fluctuation, we have further simulated the dynamics by a multiple-channel kinetic model (Figure 9). In this model, each channel contains two FRET states with FRET efficiency of ξ and 1- ξ, and each channel has a different total fluorescence intensity, $I_i = A + D$, where $i = 1, 2, ...$, and A and D are the fluorescence intensity of acceptor and donor, respectively. We demonstrated this simulation for interpreting the intermittent LH2−LH1 fluorescence intensity fluctuation dynamics. On the basis of our simulation, we have concluded that (1) the fluctuation is due to the process of the LH2, not just photon-counting shot noise; and (2) in a natural system, the anti-correlated FRET fluctuation is stochastically overshadowed by other types of correlated fluctuations, such as thermally induced spectral fluctuation, fluctuation due to phtobleaching of LH2 and LH1, and homo-energy-transfer among LH2 proteins.

The energy transfer efficiency change between donor and acceptor causes the A and D intensity fluctuation, and the fluctuation is anti-correlated, that is, donor intensity decreases while acceptor intensity increases, or vise versa. For an anti-correlated fluctuation, the cross-correlation function of donor intensity and acceptor intensity trajectory has negative amplitude that decays from a negative value to 0. However, in a complex native photosynthetic membrane, there are other factors causing the intensity fluctuations. For example, intensity jumps or blinking due to thermally induced spectral fluctuation or photophysical quenching can cause fluorescence intensity fluctuation, and LH2−LH2 energy-transfer-induced intensity fluctuation. These types of intensity changes give positive amplitude in the correlation function. If both energy transfer and blinking coexist, the sign of the amplitude is determined by whichever factor dominates at a time stochastically. When we analyzed our two-band intensity trajectories in full time length from laser on to photobleaching, we found that most molecules showed positive correlation amplitude in their fluorescence intensity correlation function, suggesting blinking dominates the intensity fluctuation, although the positive correlation amplitude does not necessarily suggest the energy transfer process as nonexist, but could simply reflect that the energy transfer under high background of thermally induced spectral fluctuation cannot be revealed by conventional correlation analysis.[21−24]

We have used fluorescence intensity fluctuations simulated by (a) a two-state hopping model with first-order kinetics and (b) the Lévy flight diffusion model.[25−31] Only the Lévy flight model can essentially simulate the features of the observed 2-D cross-correlation amplitude distributions. Although models based on more sophisticated mechanisms can also simulate the spectral fluctuation kinetics of single photosynthetic membrane fragments, the Lévy flight model catches the essential characteristics of the spectral fluctuations: smaller fluctuation steps combined with rare large jumps (Figure 10). The possible physical nature of the Lévy flight thermally induced spectral fluctuation is that the anti-correlated intensity fluctuation is due to the energy transfer among LH2 and LH1 proteins, and the auto-correlated spectral intensity jumps are due to the light-harvesting protein environment thermal fluctuations.

The single vesicle fluorescence intensity fluctuation is a complex process involving multiple states and photophysical factors (Figure 9). To simulate the fluctuation dynamics on the basis of the Lévy flight, we used the probability distribution function,

$$p(x) = \frac{1}{\pi(1 + x^2)}$$

where $p(x)$ is the probability of the system at x, and x represents fluorescence intensity states in our simulation. A Lévy flight intensity trajectory is shown in Figure 10. Comparing to normal distribution given by Brownian diffusion (Figure 10, inset), Lévy flight diffusion is heavily tailed with an infinite variance,[25−31] and it simulates well the single membrane fragment fluorescence intensity fluctuations, because our experimental data show that an intensity trajectory usually contains many small jumps and a few very large jumps. The photon-counting shot noise is not simulated here so that the behavior of Lévy flight behavior can be clearly shown. To simulate the energy transfer process, we choose to use bimodal distribution of energy transfer efficiency of ξ and $1 - \xi$. The donor and acceptor intensity trajectories based on the calculated Lévy flight (Figure 10) and switching energy transfer efficiency of $\xi = 0.488$ are shown in Figure 11A. The two-band trajectories show anti-correlated behavior

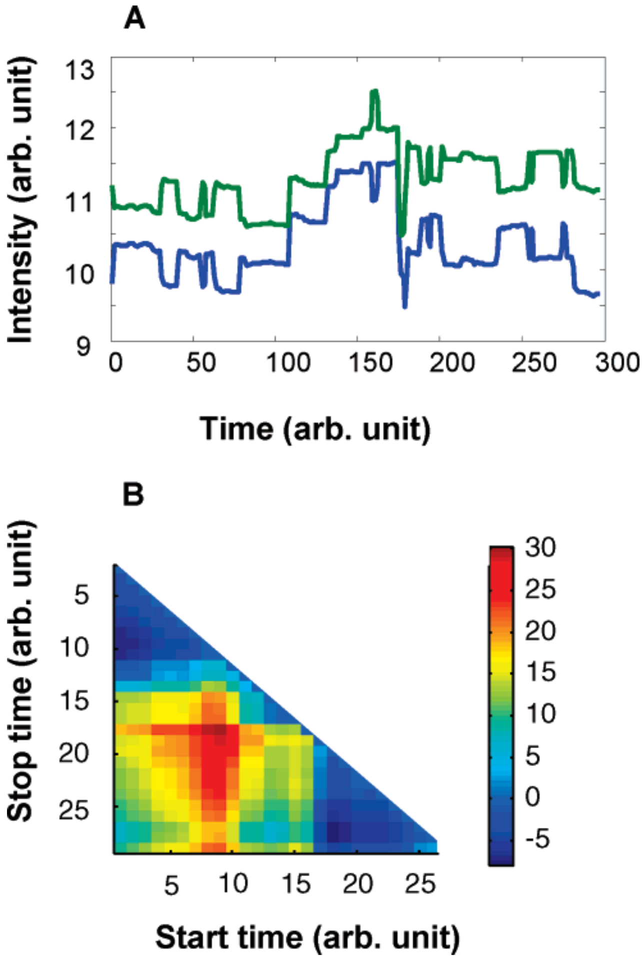

Figure 11. Two-dimension cross-correlation function amplitude mapping analysis of a pair of simulated LH2−LH1 emission trajectories. (A) A portion of a pair of LH1 and LH2 fluorescence intensity trajectories simulated by the kinetic model in Figure 9. The total intensity fluctuation is simulated by Lévy flight. The anti-correlated intensity jumps simulating the FRET efficiency change in first-order kinetics. (B) The two-dimension, cross-correlation function amplitude distribution calculated from trajectories in A. The hot color represents positive amplitude, and the cold color represents negative amplitude.

due to energy transfer efficiency change. However, this anti-correlated fluctuation is intrigued by large amplitude of correlated fluctuation due to thermally induced spectral fluctuation. Subsequently, the cross-correlation function of donor and acceptor intensities is calculated in varied and scanning time windows defined by t_{start} to t_{stop}. The 2-D amplitude distribution of the cross-correlation function is shown in Figure 11B. It is obvious that in the time window at a certain time (t_{start}) and width (from t_{start} to t_{stop}), the amplitude of cross-correlation function is negative, whereas in the whole time window, the amplitude is positive. This is simply because there are some large intensity jumps contributing to the correlation amplitude. If the time window is chosen in a relatively smaller fluctuation region, the anti-correlated spectral fluctuation associated with energy transfer can then be detected. In nature, thermally induced fluctuation is always present. The intermittent appearance of anti-crosscorrelation domains in the 2-D cross-correlation amplitude distribution indicates the fluorescence energy transfer is not always the dominating spectral behavior, and it is often buried under overall thermally induced spectral fluctuations reflected by auto-crosscorrelation positive amplitude.

We note that our identification of intermittent FRET fluctuations is more qualitative than quantitative at the present stage. Normally, if thermally induced correlated fluctuation and FRET-induced anti-correlated fluctuation are at a similar time scale, the cross-correlation amplitudes cancel each other, and only the larger amplitude component will be revealed. Because thermally induced fluctuation involves multiple complex processes, the time scale has a broad range. Therefore, only when the FRET fluctuation amplitude is larger than that of the thermal processes can anti-correlated behavior be detected. However, we found that FRET fluctuation does not always have a large amplitude. The novelty of 2-D cross-correlation amplitude mapping is the ability to search for the moments when the FRET fluctuation is large. Here, we only demonstrate that in our experimental data can the high amplitude FRET fluctuation be spotted. We emphasize that our 2-D cross-correlation amplitude mapping analysis has a more general implication for photosynthetic membranes and analyzing FRET anti-correlated donor−acceptor intensity fluctuation under a high background of other types of correlated or random fluctuations, including thermally induced intensity fluctuations, fluctuation due to photobleaching of LH2 and LH1 proteins, LH2−LH2 homo-energy-transfer- and -quenching-induced intensity fluctuations, and intensity fluctuations due to the cross-talking in detecting the donor−acceptor two-channel intensity trajectories.

It is intriguing that the spectral fluctuation can be observed at a single membrane fragment containing about 130 LH2 proteins and a number of LH1 proteins. This observation may suggest that the LH2 and LH1 proteins are not optically isolated but, rather, coupled in a certain degree, because if each protein spectrum fluctuates stochastically, the overall fluctuation should have been averaged out. However, further experiments are needed to specifically evaluate any possible topographic and spectroscopic coupling among LH2 proteins, which is beyond the scope of this work.

Conclusions

The energetic coupling among the LH1 and LH2 protein assembly determines the light-harvesting function and efficiency of the photosynthetic membranes. The light-harvesting complex assembly under ambient conditions involves dynamic intermolecular structural fluctuations that subsequently disturb the degree of energy transfer coupling between proteins in the membrane. Such intrinsic and dynamic heterogeneity plays a critical role in regulating the light-harvesting efficiency of photosynthetic membranes and offers an understanding on photon conversion efficiency of the photosynthetic membranes. Nevertheless, the spectral fluctuation we have observed by single-fragment of membrane fluorescence imaging cannot be observed by conventional ensemble-averaged spectroscopic measurements.

Acknowledgment. H.P.L. acknowledges the support from the Office of Basic Energy Sciences within the Office of Science of the U.S. Department of Energy (DOE) (Grant DE-FG02-06ER15827) and from the Office of Science of DARPA (Grants W911NF-06-1-0337). S.K. acknowledges support from NIH (Grant GM15590).

References and Notes

(1) Bahatyrova, S.; Frese, R. N.; Siebert, C. A.; Olsen, J. D.; van der Werf, K. O.; van Grondelle, R.; Niederman, R. A.; Bullough, P. A.; Otto, C.; Hunter, C. N. *Nature* **2004**, *430*, 1058.

(2) McDermott, G.; Prince, S. M.; Freer, A. A.; Hawthornthwaitelawless, A. M.; Papiz, M. Z.; Cogdell, R. J.; Isaacs, N. W. *Nature* **1995**, *374*, 517.

(3) Brixner, T.; Stenger, J.; Vaswani, H. M.; Cho, M.; Blankenship, R. E.; Fleming, G. R. *Nature* **2005**, *434*, 625.
(4) Scheuring, S.; Seguin, J.; Marco, S.; Levy, D.; Breyton, C.; Robert, B.; Rigaud, J. L. *J. Mol. Biol.* **2003**, *325*, 569.
(5) Sundstrom, V.; Pullerits, T.; van Grondelle, R. *J. Phys. Chem. B* **1999**, *103*, 2327.
(6) Fleming, G. R.; vanGrondelle, R. *Curr. Opin. Struct. Biol.* **1997**, *7*, 738.
(7) Hu, X. C.; Damjanovic, A.; Ritz, T.; Schulten, K. *Proc. Natl. Acad. Sci. U.S.A.* **1998**, *95*, 5935.
(8) Jang, S. J.; Silbey, R. J. *J. Chem. Phys.* **2003**, *118*, 9324.
(9) Nagarajan, V.; Parson, W. W. *Biochemistry* **1997**, *36*, 2300−2306.
(10) Bopp, M. A.; Jia, Y. W.; Li, L. Q.; Cogdell, R. J.; Hochstrasser, R. M. *Proc. Natl. Acad. Sci. U.S.A.* **1997**, *94*, 10630.
(11) Bopp, M. A.; Sytnik, A.; Howard, T. D.; Cogdell, R. J.; Hochstrasser, R. M. *Proc. Natl. Acad. Sci. U.S.A.* **1999**, *96*, 11271.
(12) Rutkauskas, D.; Novoderezhkin, V.; Cogdell, R. J.; van Grondelle, R. *Biophys. J.* **2005**, *88*, 422.
(13) van Oijen, A. M.; Ketelaars, M.; Kohler, J.; Aartsma, T. J.; Schmidt, J. *Science* **1999**, *285*, 400.
(14) Hu, D. H.; Lu, H. P. *J. Phys. Chem. B* **2003**, *107*, 618.
(15) Lu, H. P. *Acc. Chem. Res.* **2005**, *38*, 557.
(16) Eraso, J. M.; Kaplan, S. *Biochemistry* **2000**, *39*, 2052.
(17) Zeng, X.; Choudhary, M.; Kaplan, S. *J. Bacteriol.* **2003**, *185*, 6171.
(18) Gong, L.; Kaplan, S. *Microbiol.* **1996**, *142*, 2057.
(19) Hu, D. H.; Lu, H. P. *J. Phys. Chem. B* **2003**, *107*, 618.
(20) Tan, X.; Nalbant, P.; Toutchkine, A.; Hu, D. H.; Vorpagel, E. R.; Hahn, K. M.; Lu, H. P. *J. Phys. Chem. B* **2004**, *108*, 737.
(21) Lu, H. P.; Xun, L.; Xie, X. S. *Science* **1998**, *282*, 1877.
(22) Lu, H. P.; Xie, X. S. *Nature* **1997**, *385*, 143.
(23) For a review, see: Zwanzig, R. *Acc. Chem. Res.* **1990**, *23*, 148.
(24) van Kampen, N. G. *Stochastic Processes in Physics and Chemistry*; Elsevier: Amsterdam, Netherlands, 1992.
(25) Shlesinger, M. F.; Zaslavsky, G. M.; Klafter, J. *Nature* **1993**, *363*, 31.
(26) Klafter, J.; Shlesinger, M. F.; Zumofen, G. *Phys. Today* **1996**, *49*, 33.
(27) P. Lévy, *Théorie de l'Addition des Variables Alétories; Gauthier-Villars,: Paris, 1937.*
(28) Klafter, J.; Zumofen, G. *Physica A* **1993**, *196 A*, 102.
(29) Zumofen, G.; Klafter, J. *Phys. Rev. E: Stat. Phys., Plasmas, Fluids, Relat. Interdiscip. Top.* **1993**, *47*, 851.
(30) Geisel, T.; Thomae, S. *Phys. Rev. Lett.* **1984**, *52*, 1936.
(31) Margolin, G.; Barki, E. *J. Stat. Phys.* **2006**, *122*, 137.